World Journal of Radiology

Submit a Manuscript: http://www.wjgnet.com/esps/ *World J Radiol* 2017 March 28; 9(3): 134-142

DOI: 10.4329/wjr.v9.i3.134 ISSN 1949-8470 (online)

ORIGINAL ARTICLE

Observational Study

Multimodality imaging using proton magnetic resonance spectroscopic imaging and ^{18}F-fluorodeoxyglucose-positron emission tomography in local prostate cancer

Amita Shukla-Dave, Cecilia Wassberg, Darko Pucar, Heiko Schöder, Debra A Goldman, Yousef Mazaheri, Victor E Reuter, James Eastham, Peter T Scardino, Hedvig Hricak

Amita Shukla-Dave, Heiko Schöder, Yousef Mazaheri, Hedvig Hricak, Department of Radiology, Memorial Sloan-Kettering Cancer Center, New York, NY 10065, United States

Amita Shukla-Dave, Yousef Mazaheri, Department of Medical Physics, Memorial Sloan-Kettering Cancer Center, New York, NY 10065, United States

Cecilia Wassberg, Department of Diagnostic Radiology, Karolinska University Hospital, 17176 Solna, Sweden

Darko Pucar, Department of Radiology, Augusta University, Augusta, GA 30912, United States

Debra A Goldman, Department of Epidemiology-Biostatistics, Memorial Sloan-Kettering Cancer Center, New York, NY 10065, United States

Victor E Reuter, Department of Pathology, Memorial Sloan-Kettering Cancer Center, New York, NY 10065, United States

James Eastham, Peter T Scardino, Department of Urology, Memorial Sloan-Kettering Cancer Center, New York, NY 10065, United States

Author contributions: Shukla-Dave A, Wassberg C, Pucar D, Schöder H, Mazaheri Y and Hricak H designed the study, performed MRI and PET research, analyzed the data and wrote the paper; Goldman DA performed the statistical analysis; Reuter VE performed the pathology assessment for the study; Eastham J and Scardino PT enrolled patients, and performed clinical assessment as per standard of care; all authors reviewed the final manuscript.

Supported by National Institutes of Health grant, No. #R01 CA76423; and in part through the NIH/NCI Cancer Center Support grant, No. P30 CA008748.

Institutional review board statement: Our study was compliant with the Health Insurance Portability and Accountability Act. Twenty-two patients who were referred from the Urology department for endorectal MRI/MRSI examinations and ^{18}F-FDG-PET/CT and then underwent prostatectomy as primary or salvage treatment were included in the study.

Informed consent statement: Patient data were collected and handled in accordance with institutional and federal guidelines.

Conflict-of-interest statement: All authors have no conflicts of interest with regard to this manuscript.

Data sharing statement: Upon formal request and with proper motivation, all original data in anonymized format is available from the corresponding author for local inspection, but cannot leave Memorial Sloan Kettering Cancer Center.

Manuscript source: Invited manuscript

Correspondence to: Amita Shukla-Dave, PhD, Department of Medical Physics, Memorial Sloan-Kettering Cancer Center, 1275 York Avenue, New York, NY 10065, United States. davea@mskcc.org
Telephone: +1-212-6393184
Fax: +1-212-7173010

Received: October 31, 2016
Peer-review started: November 2, 2016
First decision: December 15, 2016
Revised: December 22, 2016
Accepted: January 11, 2017
Article in press: January 14, 2017
Published online: March 28, 2017

Abstract

AIM

To assess the relationship using multimodality imaging between intermediary citrate/choline metabolism as seen on proton magnetic resonance spectroscopic imaging (^{1}H-MRSI) and glycolysis as observed on ^{18}F-fluorodeoxyglucose positron emission tomography/computed tomography (^{18}F-FDG-PET/CT) in prostate cancer (PCa) patients.

METHODS

The study included 22 patients with local PCa who were referred for endorectal magnetic resonance imaging/^{1}H-MRSI (April 2002 to July 2007) and ^{18}F-FDG-PET/CT and then underwent prostatectomy as primary or salvage treatment. Whole-mount step-section pathology was used as the standard of reference. We assessed the relationships between PET parameters [standardized uptake value (SUVmax and SUVmean)] and MRSI parameters [choline + creatine/citrate (CC/Cmax and CC/Cmean) and total number of suspicious voxels] using spearman's rank correlation, and the relationships of PET and ^{1}H-MRSI index lesion parameters to surgical Gleason score.

RESULTS

Abnormal intermediary metabolism on ^{1}H-MRSI was present in 21/22 patients, while abnormal glycolysis on ^{18}F-FDG-PET/CT was detected in only 3/22 patients. Specifically, index tumor localization rates were 0.95 (95%CI: 0.77-1.00) for ^{1}H-MRSI and 0.14 (95%CI: 0.03-0.35) for ^{18}F-FDG-PET/CT. Spearman rank correlations indicated little relationship (ρ = -0.36-0.28) between ^{1}H-MRSI parameters and ^{18}F-FDG-PET/CT parameters. Both the total number of suspicious voxels (ρ = 0.55, P = 0.0099) and the SUVmax (ρ = 0.46, P = 0.0366) correlated weakly with the Gleason score. No significant relationship was found between the CC/Cmax, CC/Cmean or SUVmean and the Gleason score (P = 0.15-0.79).

CONCLUSION

The concentration of intermediary metabolites detected by ^{1}H MRSI and glycolytic flux measured ^{18}F-FDG PET show little correlation. Furthermore, only few tumors were FDG avid on PET, possibly because increased glycolysis represents a late and rather ominous event in the progression of PCa.

Key words: Proton magnetic resonance spectroscopic imaging; ^{18}F-fluorodeoxyglucose-positron emission tomography; Prostate cancer

Core tip: Although metabolic imaging is increasingly utilized in prostate cancer (PCa), the mechanisms leading to cancer-related metabolic rearrangements and consequent imaging findings remain poorly understood. This study compared two modalities utilizing distinct metabolic pathways, proton magnetic resonance spectroscopic imaging (^{1}H-MRSI) and ^{18}F-fluorodeoxyglucose positron emission tomography/computed tomography (^{18}F-FDG-PET/CT), in local PCa. Abnormal intermediary metabolism on ^{1}H-MRSI was present in 21/22 patients, while abnormal glycolysis on ^{18}F-FDG-PET/CT was detected in only 3/22 patients. This study provides an insight why metabolic PET agents promising for detection of PCa target intermediary metabolism. On the other hand, elevated glycolysis may have ominous prognostic implications in PCa.

Shukla-Dave A, Wassberg C, Pucar D, Schöder H, Goldman DA, Mazaheri Y, Reuter VE, Eastham J, Scardino PT, Hricak H. Multimodality imaging using proton magnetic resonance spectroscopic imaging and ^{18}F-fluorodeoxyglucose-positron emission tomography in local prostate cancer. *World J Radiol* 2017; 9(3): 134-142 Available from: URL: http://www.wjgnet.com/1949-8470/full/v9/i3/134.htm DOI: http://dx.doi.org/10.4329/wjr.v9.i3.134

INTRODUCTION

Multimodality imaging is performed in patients with cancer to understand metabolism, however the mechanisms leading to metabolic rearrangements remains poorly understood. By decoding the connections between cancer signaling and metabolism, it may be possible to better understand the clinical implications of imaging findings and develop new imaging strategies.

In patients with prostate cancer (PCa), two key functional imaging modalities, proton magnetic resonance spectroscopic imaging (^{1}H-MRSI) and ^{18}F-fluorodeoxyglucose positron emission tomography/computed tomography (^{18}F-FDG-PET/CT), are used to identify cancer-induced changes in cellular metabolism[1-3]. On ^{1}H-MRSI, decreased levels of citrate (a Krebs cycle and fatty acid synthesis intermediate) and polyamines (amino acid metabolism intermediates) and elevated choline (a precursor of membrane synthesis) are a signature of PCa[2,4-7]. On ^{18}F-FDG-PET, increased glucose uptake by glucose transporters and glucose phosphorylation to glucose-6-phosphate by hexokinase are used for identifying PCa and other cancers[3,8]. The indications for ^{1}H-MRSI and ^{18}F-FDG-PET/CT examinations in patients with PCa are very different[9,10]. ^{1}H-MRSI adds incremental value to standard prostate magnetic resonance imaging (MRI) in the detection of primary or recurrent loco-regional PCa and in the evaluation of its aggressiveness (Gleason Grade)[9-14]. ^{1}H-MRSI can also be used prior to treatment to predict biochemical relapse of PCa after radical prostatectomy or the presence of insignificant PCa[14-17]. In contrast, ^{18}F-FDG-PET/CT is not recommended for the detection and initial evaluation of PCa or detection of early recurrence. Various other PET agents, such as ^{18}F- or ^{11}C-labeled choline or acetate, several various amino acids, and agents binding to the

transmembrane PSMA molecule are available for this purpose[18-24]. ^{18}F-FDG plays a role in the characterization of advanced metastatic PCa[8,25]. The clinical significance of the current study lies in exploring the use of multimodality imaging in local PCa. In this study, we wanted to explore the relationship using multimodality imaging between concentrations of intermediary metabolites citrate and choline, measured by ^{1}H-MRSI, and glycolysis as noted on ^{18}F-FDG PET/CT in local PCa.

MATERIALS AND METHODS

Patient demographics

Our study was compliant with the Health Insurance Portability and Accountability Act. Patient data were collected and handled in accordance with institutional and federal guidelines. Twenty-two patients who were referred from the Urology department for endorectal MRI/MRSI examinations (April 2002 to July 2007) and ^{18}F-FDG-PET/CT and then underwent prostatectomy as primary or salvage treatment were included in the study. Whole-mount step-section pathology of the surgical specimen was available for all the patients. Of the 22 patients, 11 were imaged before treatment while 11 were imaged after external beam radiation therapy. The institutional review board approved our retrospective review of multimodality imaging using MRI/MRSI and ^{18}F-FDG-PET/CT studies, pathology data (from surgical pathology), and clinical follow-up data and waived the informed consent requirement. The mean time between the MRSI and PET exams was 11 ± 37 d (± SD).

Endorectal MRI/MRSI data acquisition and processing

Data were acquired on a 1.5-Tesla GE Signa Horizon scanner. MRI was done using a pelvic phased-array coil and an expandable endorectal coil; T1- and T2-weighted spin-echo MR images were obtained using a previously described standard prostate imaging protocol (total time, approximately 30 min)[4]. MR image acquisition was followed by a standard MRSI protocol with point-resolved spectroscopic voxel excitation and water and lipid suppression (total time, 17 min) in a voxel array and the SI dimension zero filled to 16 slices (3-mm resolution) with a voxel size of 0.12 to 0.16 cm^3[4]. MRSI data were overlaid on the corresponding T2-weighted images, including the raw spectra and the metabolic ratio [choline + creatine to citrate (CC/C)][4]. Tumors were identified by dedicated radiologists with > 5 years of experience in prostate imaging.

^{1}H-MRSI data interpretation

An MRI physicist with > 10 years of experience in prostate MRSI retrospectively interpreted the ^{1}H-MRSI studies using established metabolic criteria for the evaluation of PCa in the peripheral and transition zones[6,14,26,27]. The physicist, who was blinded to clinical data and surgical pathology, recorded the location and total number of suspicious voxels (tumor volume estimation), maximum (max) CC/C, and mean CC/C for the index lesion[6,14,26,27].

^{18}F-FDG-PET/CT data acquisition and processing

Details of the 18F-FDG-PET/CT imaging procedure have been described previously[28]. Briefly, a low-dose CT scan (120-140 kV, approximately 80 mA), which is used for attenuation correction of PET emission images as well as for anatomic localization of PET abnormalities, was acquired first. This was followed by acquisition of PET emission images of the lower pelvis including of the prostate for 5 min per bed position. Images were reconstructed using iterative algorithms with average slice thickness of 3 mm and a 128 × 128 matrix size. Patients were scanned in the supine position. Before the examination, patients fasted for at least 6 h, but liberal intake of water was allowed. Patients were injected intravenously with 444-555 MBq of ^{18}F-FDG and a PET/CT scan started after an uptake period of approximately 60 min. Plasma glucose level was < 200 mg at the time of imaging in all patients.

^{18}F-FDG-PET/CT data interpretation

All ^{18}F-FDG-PET/CT data were available for retrospective review on a standard clinical workstation (PACS with Advance Work Station extension; General Electric). One board-certified radiologist/nuclear medicine physician, who had > 10 years of experience in PET and > 5 years of experience in prostate imaging, reviewed the ^{18}F-FDG-PET/CT studies. PET images were analyzed in three orthogonal planes (transaxial, coronal, sagittal) both visually and quantitatively. For quantitative PET analysis, maximum standardized uptake value (SUVmax) and average SUV (SUVmean) of the index lesion were determined using a Volume of Interest with 40% threshold of SUVmax. All SUVs were normalized to body weight.

Pathology

Whole-mount transverse serial sections of the prostate were prepared as described previously[29]. The distal 5-mm portion of the apex was amputated and coned. The remainder of the gland was serially sectioned from the apex to the base at 3-4-mm intervals and submitted in its entirety for paraffin-embedded whole mounts. Cancer foci were outlined in ink on whole-mount, apical, and seminal vesicle sections and photographed. The photographs constituted the tumor maps. The primary and secondary Gleason grades as well as the pathologic tumor node stage were also determined. The index lesion was identified in all cases as the tumor with the largest volume. Tissue sections stained with H and E were examined by one uro-pathologist blinded to imaging and clinical data.

Matching of MRI/MRSI data, ^{18}F-FDG-PET/CT and pathology data

The matching of imaging and pathology for the index lesion was performed in consensus by two dually-boarded radiologists/nuclear medicine physicians with

Table 1 Patient characteristics

		n (%)
Clinical stage[1]	T1c	10 (45.5)
	T2a	4 (18.2)
	T2b	4 (18.2)
	T2c	1 (4.5)
	T3	1 (4.5)
	T3a	2 (9.1)
Biopsy Gleason score	0 + 0	1 (4.5)
	3 + 3	3 (13.6)
	3 + 4	5 (22.7)
	4 + 3	5 (22.7)
	4 + 4	4 (18.2)
	4 + 5	4 (18.2)
Pathology stage	pT2a	3 (13.6)
	pT2b	5 (22.7)
	pT3a	7 (31.8)
	pT3b	6 (27.3)
	pT4	1 (4.5)
Pathology Gleason score	3 + 3	1 (4.5)
	3 + 4	8 (36.4)
	4 + 3	4 (18.2)
	4 + 4	4 (18.2)
	4 + 5	3 (13.6)
	5 + 4	1 (4.5)
	Not Graded[2]	1 (4.5)
Prior radiation treatment	EBRT	11 (50)
	Untreated	11 (50)

[1]Clinical stage was determined prior to primary or salvage surgery; [2]One index tumor was not graded due to treatment effect. EBRT: External beam radiation therapy.

> 5 years and > 15 years of experience in prostate imaging. The histopathologic axial step sections were visually matched with corresponding axial T2-weighted transverse MR images with superimposed MRSI data and fused ^{18}F-FDG PET/CT data with a precision of ± 1 slice based on established anatomic landmarks[12]. Because the spectroscopic data were acquired in the same position and with the same gradients as the imaging data, registration of the spectroscopic data with the T2-weighted images was automatic, and the spectroscopic data could be compared with the most closely corresponding histopathologic step section.

Statistical analysis

Clinical and pathological characteristics were described using medians and ranges for continuous variables and frequencies and percents or proportions for categorical variables. Gleason grades were summed into Gleason scores of 6, 7, 8 or 9.

The localization rates of ^{18}F-FDG-PET/CT and ^{1}H-MRSI were calculated along with exact 95% confidence intervals. The relationships between PET parameters (SUVmax and SUVmean) and MRSI parameters (CC/Cmax, CC/Cmean, Total # Voxels) were assessed using Spearman's rank correlation and graphically displayed with scatter plots and 95% confidence bands. Additionally, the relationships of PET and MRSI parameters to surgical Gleason score were assessed with Spearman's rank correlation and, given the Gleason score's ordinal nature, graphically illustrated with box plots. *P*-values less than 0.05 were considered statistically significant. All analyses were done using SAS 9.4 (The SAS Institute, Cary, NC).

RESULTS

Patient characteristics are summarized in Table 1. The patients had a median age of 58 years (range: 47-70 years) and median PSA of 4.81 ng/mL (range: 0.11-96.53 ng/mL).

Index tumor localization rates were 0.95 (95%CI: 0.77-1.00) for ^{1}H-MRSI and 0.14 (95%CI: 0.03-0.35) for ^{18}F-FDG-PET/CT, with 21 out of 22 index tumors found on pathology identified on ^{1}H-MRSI and only 3 of those 21 index lesions identified on ^{18}F-FDG-PET/CT. Figure 1 shows ^{1}H-MRSI, ^{18}F-FDG-PET/CT and whole-mount step-section pathology from a patient in whom the tumor seen at pathology was observed by multimodality imaging. Figure 2 shows ^{1}H-MRSI, ^{18}F-FDG-PET/CT and whole-mount step-section pathology from a patient in whom the tumor seen at pathology was observed by ^{1}H-MRSI only. In the 3 patients with positive PET findings, the total tumor volumes measured by PET were 10.9, 11.1 and 10.4 cc and the SUVmax values were 3.3, 3.5 and 4.5. On ^{1}H-MRSI in the 21 positive patients, CC/Cmax (median 6.4, range: 0.5-37.4), CC/Cmean (median 2.0, range: 0.5-18.5) and number of suspicious voxels (median 9.0, range 2-32) showed more profound alterations for all patients. Both the scatter plots (Figure 3 and Table 2) and the Spearman rank correlations indicated little relationship between ^{1}H-MRSI parameters and ^{18}F-FDG-PET/CT. Spearman's ρ ranged between -0.362 and 0.28 (*P*-values range: 0.10-0.66). No clear pattern of association was detected in the graphs.

Gleason scores ranged from 6 (8/22, 36%) to 9 (4/22, 18.1%) with one patient lacking a score due to treatment effect. This patient was excluded from further analysis. Both the total number of voxels (ρ = 0.55, *P* = 0.0099) and the SUVmax (ρ = 0.46, *P* = 0.0366) correlated with the Gleason score. No significant relationship was found between the CC/Cmax, CC/Cmean or SUVmean and the Gleason score (*P* = 0.15-0.79, Table 3). The box plots demonstrate an upward trend for total number of voxels and SUVmax with each subsequent Gleason score (Figure 4).

DISCUSSION

Multimodality imaging in PCa detection on ^{1}H-MRSI is based on the detection of decreased citrate and polyamines with elevated choline[2,4]. This is reflected in the high CC/Cmax (median 9.0) and CC/Cmean (median: 2.0) for the prostate index lesions. On ^{18}F-FDG-PET/CT, PCa is identified based on increased glucose uptake by glucose transporters (GLUT) and glucose phosphorylation to glucose-6-phosphate by hexokinase[3,8]. The present study adds to the literature for patients with local or loco-regional primary or recurrent PCa and shows that the

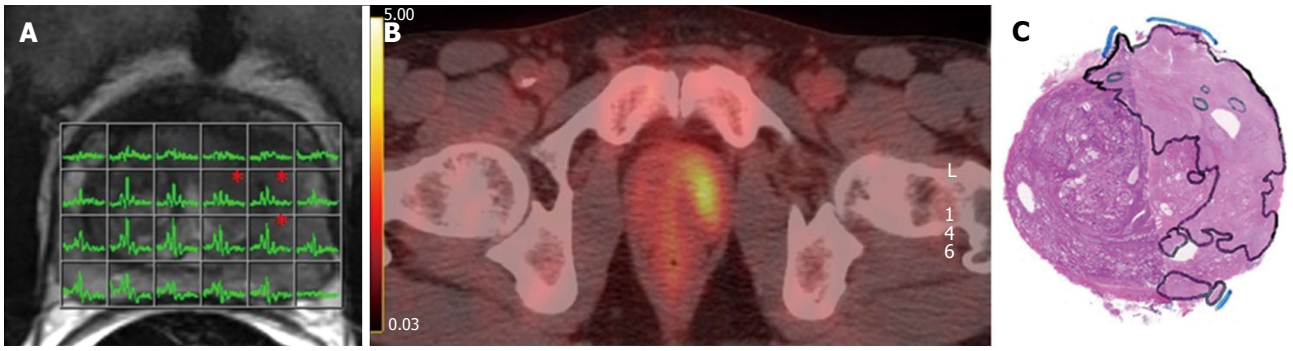

Figure 1 Representative 1.5T magnetic resonance imaging/magnetic resonance spectroscopic imaging in a 58-year-old patient with prostate specific antigen 96.53 ng/mL, clinical stage T3 and surgical Gleason score 4 + 5. A: Axial T2-weighted image and overlaid point-resolved spectroscopic box indicating excitation region selected and 3D MRSI demonstrating three suspicious voxels marked with asterisks; B: ^{18}F-FDG-PET/CT fusion image shows a focal uptake in the left prostate; C: Whole-mount step-section histopathology after radical prostatectomy shows a large cancer in the left prostate. MRSI: Magnetic resonance spectroscopic imaging; ^{18}F-FDG-PET/CT: ^{18}F-fluorodeoxyglucose positron emission tomography/computed tomography.

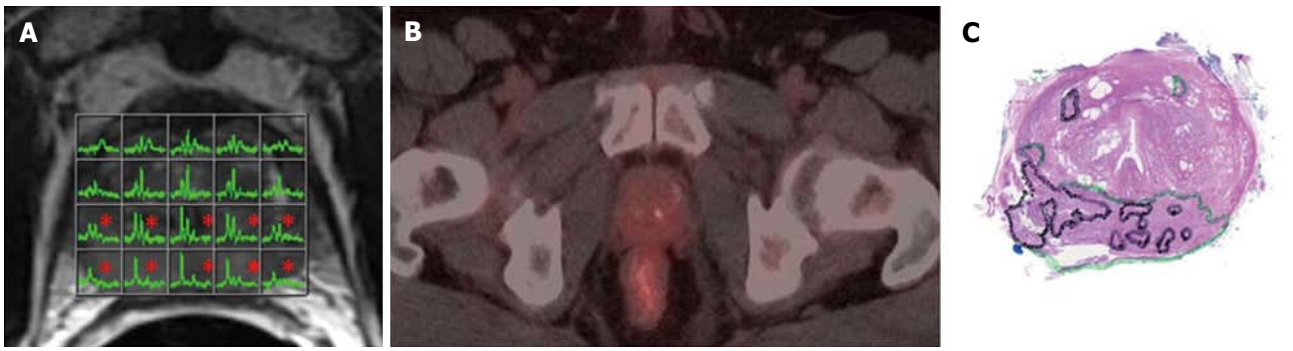

Figure 2 Representative 1.5T magnetic resonance imaging/magnetic resonance spectroscopic imaging in a 64-year-old patient with prostate specific antigen 4.9 ng/mL, clinical stage T3 and surgical Gleason score 4 + 3. A: Axial T2-weighted image and overlaid point-resolved spectroscopic box indicating excitation region selected and 3D MRSI demonstrating ten suspicious voxels marked with asterisks; B: ^{18}F-FDG-PET/CT fusion image shows no focal uptake in the prostate; C: Whole-mount step-section histopathology after radical prostatectomy shows a large cancer extending from medial to right side of the prostate. MRSI: Magnetic resonance spectroscopic imaging; ^{18}F-FDG-PET/CT: ^{18}F-fluorodeoxyglucose positron emission tomography/computed tomography.

Table 2 Spearman correlations between proton magnetic resonance spectroscopic imaging and ^{18}F-fluorodeoxyglucose data (n = 22)

^{1}H-MRSI	^{18}F-FDG	Rho (ρ)	*P*-value
CC/Cmax	SUVmax	-0.281	0.21
	SUVmean	-0.101	0.66
CC/Cmean	SUVmax	-0.362	0.10
	SUVmean	-0.158	0.48
Total # Voxels	SUVmax	0.2565	0.25
	SUVmean	0.2783	0.21

^{1}H-MRSI: Proton magnetic resonance spectroscopic imaging; ^{18}F-FDG: ^{18}F-fluorodeoxyglucose.

Table 3 Spearman correlations between proton magnetic resonance spectroscopic imaging and ^{18}F-fluorodeoxyglucose data and surgical Gleason score (n = 22)

	With Gleason score	
^{18}F-FDG/^{1}H-MRSI	Rho (ρ)	*P*-value
CC/Cmax	0.2165	0.35
CC/Cmean	0.0624	0.79
Total # Voxels	0.5493	0.0099
SUVmean	0.3225	0.15
SUVmax	0.4584	0.0366

^{1}H-MRSI: Proton magnetic resonance spectroscopic imaging; ^{18}F-FDG: ^{18}F-fluorodeoxyglucose.

citrate decrease in PCa was both much more frequent and pronounced than was the elevation in ^{18}F-FDG uptake. This is in-line with the known low sensitivity of ^{18}F-FDG-PET/CT for detecting localized primary PCa. Further research is needed to develop a clearer understanding of the underlying genomic and metabolic mechanisms and to confirm whether metabolic alterations progress stepwise from early abnormalities in citrate metabolism to late abnormalities in glucose metabolism. Since our patients were imaged at only one time point, the data appear consistent with this understanding. Improved understanding of PCa metabolism could help in determining the most appropriate imaging modalities (including imaging with radiotracers) for different clinical stages of PCa and possibly also in identifying and monitoring novel targeted therapies.

For instance, according to the "bioenergetic theory of prostate malignancy"[1,17], the normal prostate produces

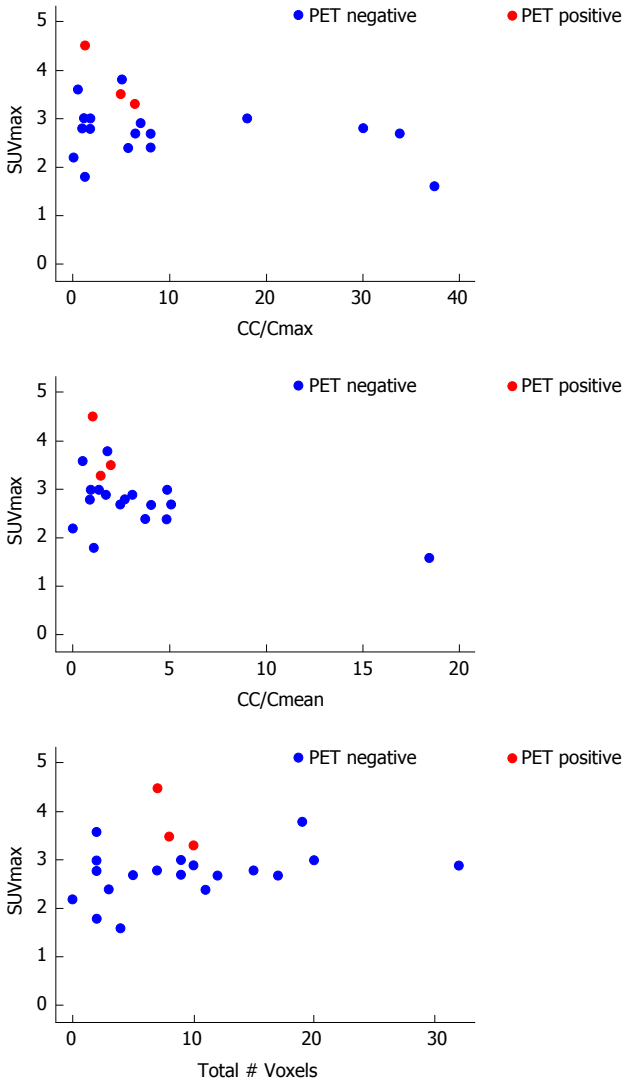

Figure 3 Scatter plots demonstrating the relationships between proton magnetic resonance spectroscopic imaging and ^{18}F-fluorodeoxyglucose positron emission tomography parameters (*n* = 22). PET: Positron emission tomography.

and secretes an enormous amount of citrate; this is achieved by zinc-induced inhibition of m-aconitase, a Krebs cycle enzyme that converts citrate to isocitrate. With this truncated Krebs cycle, the normal prostate sacrifices ATP production for citrate secretion[17]. Conversely, in PCa, down-regulation of multiple membrane zinc transporters and zinc decline lead to activation of the full Krebs cycle, oxidation and a consequent decrease in intracellular and secreted citrate and increase in ATP production supporting malignancy[30-32]. However, the decline of citrate in PCa could also be related to its conversion to AcCoA by cytosolic ATP citrate lyase (ACLY) and subsequent utilization for fatty acid synthesis[30,33,34]. Activation of ACLY seems to be critical for biosynthesis and growth in various cancer models[30,34]. Thus, based on this bioenergetic theory, two possible scenarios could explain the low ^{18}F-FDG uptake in early, slow-growing PCa: (1) early PCa exhibits only a mildly increased cellular energy demand that is matched by activation of the mitochondrial Krebs cycle (bioenergetic mode); or (2) early PCa exhibits an unchanged energy demand and retains a persistently truncated Krebs cycle, but it diverts cytosolic citrate from secretion to fatty acid synthesis (biosynthetic mode).

Biochemical alterations in PCa may be linked to signaling pathways implicated in PCa initiation and progression. For example, the PTEN/PI-3-Kinase pathway, one of the central pathways in early PCa, is closely linked to cellular metabolism[35]. PTEN tumor suppressor loss, with subsequent activation of the PI-3-Kinase pathway and downstream effectors such as AKT and mTOR[36,37], has anabolic effects leading to increased glucose and amino acid uptake for the purposes of protein, fatty acid, and membrane synthesis, as well as the expression and membrane localization of glucose transporters[38]. Other consequences of PTEN loss include hexokinase translocation to the mitochondrial membrane[39], FA synthesis *via* ACLY[40,41], steroid hormone-dependent FA synthesis[42], glycogen synthesis, membrane localization of amino-acid transporters, amino-acid uptake, and protein synthesis[43]. Other signaling alterations that typically occur later in PCa progression may also eventually upregulate glycolysis. Loss of p53, for example, is associated with increased glycolysis through GLUT3 expression[44]. We therefore summarize the following: In early PCa, citrate is diverted from secretion to AKT-dependent FA synthesis and/or to zinc-deficiency-induced oxidation in the Krebs cycle, leading to a decline in citrate signal on ^{1}H-MRSI. While AKT-dependent stimulation of glycolysis alone is insufficient to produce a detectable increase in ^{18}F-FDG uptake in PCa, the subsequent loss of p53 further promotes glycolysis, resulting in a detectable difference in ^{18}F-FDG uptake between PCa and normal prostate tissue. We are hoping that future studies which include genomic and proteomic tissue analysis, may eventually link tumor biology and imaging in PCa. Such links have been made in other studies. For instance, the extent of changes in intermediary metabolism on ^{1}H-MRSI has been shown to correlate with the Gleason grade[14]. Similarly, risk scoring based on metabolic changes on ^{1}H-MRSI has been found to correlate with treatment outcome in patients with high-risk PCa who underwent neoadjuvant chemotherapy/hormone therapy before radical prostatectomy or radiation therapy[15]. Conversely, near-normal intermediary metabolism on pre-treatment ^{1}H-MRSI has been found to predict very-low-risk PCa in radical prostatectomy specimens[16].

Certain PET tracers are superior to ^{18}F-FDG in detecting early PCa and early recurrence after radical prostatectomy or radiation therapy[18-24]. In contrast, in the most-advanced form of PCa, castration-resistant disease, ^{18}F-FDG-PET/CT is predictive of survival[28,45], supporting the statement that increased glycolysis represents a late and ominous event in the progression of PCa. Of note, ^{18}F-FDG-PET/CT has been established as predictive of outcome in multiple other cancers, with high ^{18}F-FDG avidity predicting poor outcome[46-49]. The present study

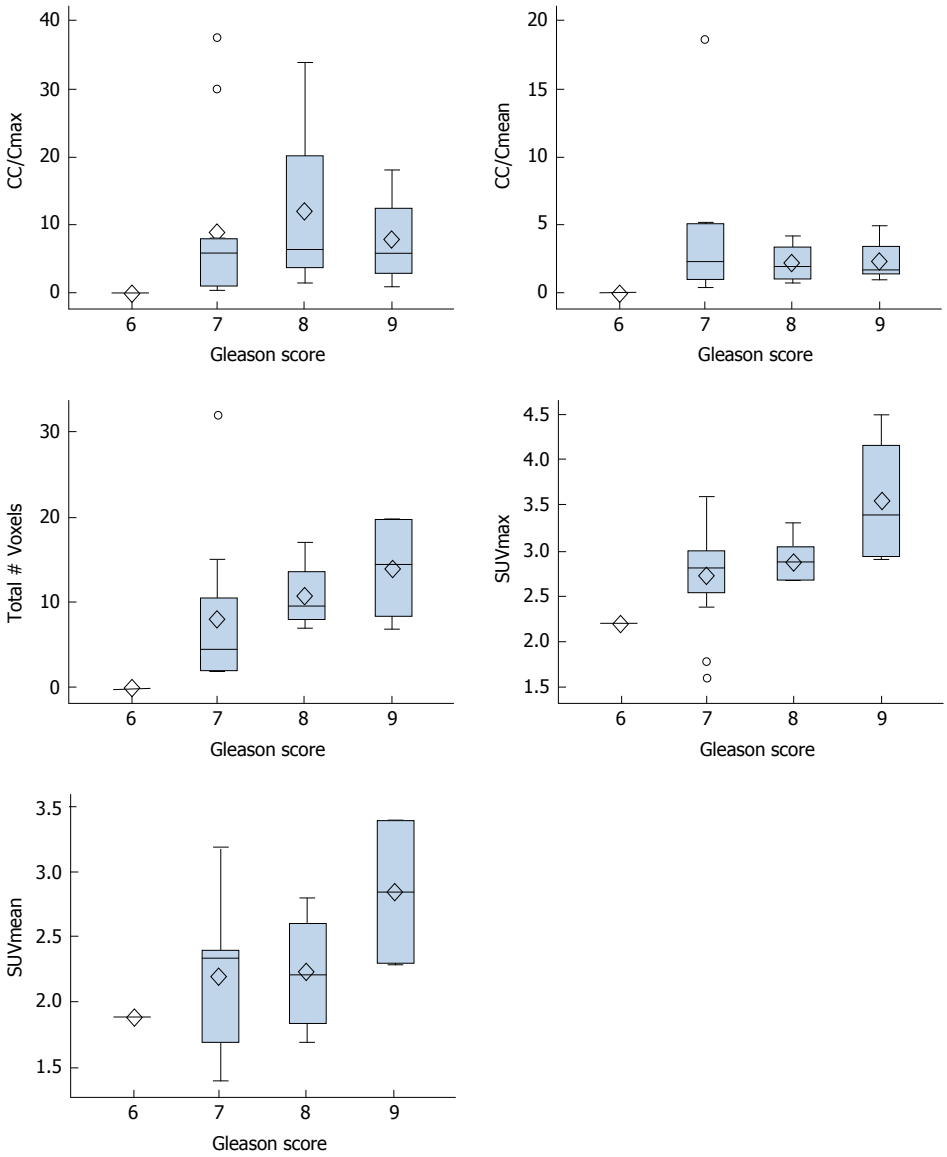

Figure 4 Box plots demonstrating the relationships between surgical Gleason score and imaging parameters (*n* = 22).

has a few limitations given its retrospective study design and the fact that we could not control for treatment. Also, due to a low sample size, it was not feasible to estimate survival. However, this study met its purpose of exploring the relationship using multimodality imaging between ^{1}H-MRSI and ^{18}F-FDG-PET/CT in PCa patients. To optimize PCa multimodality imaging, it is critical to understand how different metabolic imaging techniques interact and how they can be used to develop the most effective imaging protocols.

The present study suggests that the concentration of intermediary metabolites detected by ^{1}H MRSI and glycolytic flux measured ^{18}F-FDG PET show little correlation. Furthermore, only few tumors were FDG avid on PET, possibly because increased glycolysis represents a late and rather ominous event in the progression of PCa.

ACKNOWLEDGMENTS

The authors thank Ada Muellner, MS for editing the manuscript.

COMMENTS

Background

Although metabolic imaging is increasingly utilized in prostate cancer (PCa), the mechanisms leading to cancer-related metabolic rearrangements and consequent imaging findings remain poorly understood. The aim of the study was to better understand the sequence of metabolic changes in localized PCa.

Research frontiers

To optimize PCa multimodality imaging, it is critical to understand how different metabolic imaging techniques interact and how they can be used to develop the most effective imaging protocols.

Innovations and breakthroughs

Comparison of proton magnetic resonance spectroscopic imaging (^{1}H-MRSI) and ^{18}F-fluorodeoxyglucose positron emission tomography/computed tomography (^{18}F-FDG-PET/CT) findings in local PCa demonstrated that abnormal choline intermediary metabolism on ^{1}H-MRSI precedes the changes in glycolysis on ^{18}F-FDG-PET/CT.

Applications

In principle, imaging analysis of distinct metabolic pathways in PCa can be utilized to predict patient outcome, optimize management, and plan future

diagnostic and therapeutic trials in PCa.

Terminology

^{1}H-MRSI: Proton magnetic resonance spectroscopic imaging; ^{18}F-FDG-PET: ^{18}F-FDG-positron emission tomography; PCa: Prostate cancer.

Peer-review

The topic is actual and interesting.

REFERENCES

1 **Costello LC**, Franklin RB. Citrate metabolism of normal and malignant prostate epithelial cells. *Urology* 1997; **50**: 3-12 [PMID: 9218011 DOI: 10.1016/S0090-4295(97)00124-6]

2 **Kurhanewicz J**, Vigneron DB, Hricak H, Narayan P, Carroll P, Nelson SJ. Three-dimensional H-1 MR spectroscopic imaging of the in situ human prostate with high (0.24-0.7-cm3) spatial resolution. *Radiology* 1996; **198**: 795-805 [PMID: 8628874]

3 **Schöder H**, Larson SM. Positron emission tomography for prostate, bladder, and renal cancer. *Semin Nucl Med* 2004; **34**: 274-292 [PMID: 15493005]

4 **Shukla-Dave A**, Hricak H, Moskowitz C, Ishill N, Akin O, Kuroiwa K, Spector J, Kumar M, Reuter VE, Koutcher JA, Zakian KL. Detection of prostate cancer with MR spectroscopic imaging: an expanded paradigm incorporating polyamines. *Radiology* 2007; **245**: 499-506 [PMID: 17890357 DOI: 10.1148/radiol.2452062201]

5 **Swanson MG**, Vigneron DB, Tabatabai ZL, Males RG, Schmitt L, Carroll PR, James JK, Hurd RE, Kurhanewicz J. Proton HR-MAS spectroscopic and quantitative pathologic analysis of MRI/3D-MRSI-targeted postsurgical prostate tissues. *Magn Reson Med* 2003; **50**: 944-954 [PMID: 14587005]

6 **Mazaheri Y**, Shukla-Dave A, Muellner A, Hricak H. MRI of the prostate: clinical relevance and emerging applications. *J Magn Reson Imaging* 2011; **33**: 258-274 [PMID: 21274967 DOI: 10.1002/jmri.22420]

7 **Sciarra A**, Barentsz J, Bjartell A, Eastham J, Hricak H, Panebianco V, Witjes JA. Advances in magnetic resonance imaging: how they are changing the management of prostate cancer. *Eur Urol* 2011; **59**: 962-977 [PMID: 21367519 DOI: 10.1016/j.eururo.2011.02.034]

8 **Schöder H**, Herrmann K, Gönen M, Hricak H, Eberhard S, Scardino P, Scher HI, Larson SM. 2-[18F]fluoro-2-deoxyglucose positron emission tomography for the detection of disease in patients with prostate-specific antigen relapse after radical prostatectomy. *Clin Cancer Res* 2005; **11**: 4761-4769 [PMID: 16000572 DOI: 10.1158/1078-0432.CCR-05-0249]

9 **Hricak H**, Choyke PL, Eberhardt SC, Leibel SA, Scardino PT. Imaging prostate cancer: a multidisciplinary perspective. *Radiology* 2007; **243**: 28-53 [PMID: 17392247]

10 **Pucar D**, Sella T, Schöder H. The role of imaging in the detection of prostate cancer local recurrence after radiation therapy and surgery. *Curr Opin Urol* 2008; **18**: 87-97 [PMID: 18090496]

11 **Yu KK**, Scheidler J, Hricak H, Vigneron DB, Zaloudek CJ, Males RG, Nelson SJ, Carroll PR, Kurhanewicz J. Prostate cancer: prediction of extracapsular extension with endorectal MR imaging and three-dimensional proton MR spectroscopic imaging. *Radiology* 1999; **213**: 481-488 [PMID: 10551230 DOI: 10.1148/radiology.213.2.r99nv26481]

12 **Pucar D**, Shukla-Dave A, Hricak H, Moskowitz CS, Kuroiwa K, Olgac S, Ebora LE, Scardino PT, Koutcher JA, Zakian KL. Prostate cancer: correlation of MR imaging and MR spectroscopic with pathologic findings after radiation therapy-initial experience. *Radiology* 2005; **236**: 545-553 [PMID: 15972335 DOI: 10.1148/radiol.2362040739]

13 **Wefer AE**, Hricak H, Vigneron DB, Coakley FV, Lu Y, Wefer J, Mueller-Lisse U, Carroll PR, Kurhanewicz J. Sextant localization of prostate cancer: comparison of sextant biopsy, magnetic resonance imaging and magnetic resonance spectroscopic imaging with step section histology. *J Urol* 2000; **164**: 400-404 [PMID: 10893595]

14 **Zakian KL**, Sircar K, Hricak H, Chen HN, Shukla-Dave A, Eberhardt S, Muruganandham M, Ebora L, Kattan MW, Reuter VE, Scardino PT, Koutcher JA. Correlation of proton MR spectroscopic imaging with gleason score based on step-section pathologic analysis after radical prostatectomy. *Radiology* 2005; **234**: 804-814 [PMID: 15734935 DOI: 10.1148/radiol.2343040363]

15 **Pucar D**, Koutcher JA, Shah A, Dyke JP, Schwartz L, Thaler H, Kurhanewicz J, Scardino PT, Kelly WK, Hricak H, Zakian KL. Preliminary assessment of magnetic resonance spectroscopic imaging in predicting treatment outcome in patients with prostate cancer at high risk for relapse. *Clin Prostate Cancer* 2004; **3**: 174-181 [PMID: 15636684]

16 **Shukla-Dave A**, Hricak H, Kattan MW, Pucar D, Kuroiwa K, Chen HN, Spector J, Koutcher JA, Zakian KL, Scardino PT. The utility of magnetic resonance imaging and spectroscopic for predicting insignificant prostate cancer: an initial analysis. *BJU Int* 2007; **99**: 786-793 [PMID: 17223922]

17 **Costello LC**, Franklin RB. The clinical relevance of the metabolism of prostate cancer; zinc and tumor suppression: connecting the dots. *Mol Cancer* 2006; **5**: 17 [PMID: 16700911]

18 **Breeuwsma AJ**, Rybalov M, Leliveld AM, Pruim J, de Jong IJ. Correlation of [11C]choline PET-CT with time to treatment and disease-specific survival in men with recurrent prostate cancer after radical prostatectomy. *Q J Nucl Med Mol Imaging* 2012; **56**: 440-446 [PMID: 23069923]

19 **Giovacchini G**, Picchio M, Garcia-Parra R, Briganti A, Abdollah F, Gianolli L, Schindler C, Montorsi F, Messa C, Fazio F. 11C-choline PET/CT predicts prostate cancer-specific survival in patients with biochemical failure during androgen-deprivation therapy. *J Nucl Med* 2014; **55**: 233-241 [PMID: 24408897 DOI: 10.2967/jnumed.113.123380]

20 **Kwee SA**, Lim J, Watanabe A, Kromer-Baker K, Coel MN. Prognosis Related to Metastatic Burden Measured by ^{18}F-Fluorocholine PET/CT in Castration-Resistant Prostate Cancer. *J Nucl Med* 2014; **55**: 905-910 [PMID: 24676753 DOI: 10.2967/jnumed.113.135194]

21 **Morris MJ**, Scher HI. (11)C-acetate PET imaging in prostate cancer. *Eur J Nucl Med Mol Imaging* 2007; **34**: 181-184 [PMID: 17238014 DOI: 10.1007/s00259-006-0281-5]

22 **Nuñez R**, Macapinlac HA, Yeung HW, Akhurst T, Cai S, Osman I, Gonen M, Riedel E, Scher HI, Larson SM. Combined 18F-FDG and 11C-methionine PET scans in patients with newly progressive metastatic prostate cancer. *J Nucl Med* 2002; **43**: 46-55 [PMID: 11801702]

23 **Ren J**, Yuan L, Wen G, Yang J. The value of anti-1-amino-3-18F-fluorocyclobutane-1-carboxylic acid PET/CT in the diagnosis of recurrent prostate carcinoma: a meta-analysis. *Acta Radiol* 2016; **57**: 487-493 [PMID: 25907118 DOI: 10.1177/0284185115581541]

24 **Turkbey B**, Mena E, Shih J, Pinto PA, Merino MJ, Lindenberg ML, Bernardo M, McKinney YL, Adler S, Owenius R, Choyke PL, Kurdziel KA. Localized prostate cancer detection with 18F FACBC PET/CT: comparison with MR imaging and histopathologic analysis. *Radiology* 2014; **270**: 849-856 [PMID: 24475804 DOI: 10.1148/radiol.13130240]

25 **Cimitan M**, Bortolus R, Morassut S, Canzonieri V, Garbeglio A, Baresic T, Borsatti E, Drigo A, Trovò MG. [18F]fluorocholine PET/CT imaging for the detection of recurrent prostate cancer at PSA relapse: experience in 100 consecutive patients. *Eur J Nucl Med Mol Imaging* 2006; **33**: 1387-1398 [PMID: 16865395]

26 **Shukla-Dave A**, Hricak H, Eberhardt SC, Olgac S, Muruganandham M, Scardino PT, Reuter VE, Koutcher JA, Zakian KL. Chronic prostatitis: MR imaging and 1H MR spectroscopic imaging findings--initial observations. *Radiology* 2004; **231**: 717-724 [PMID: 15163811 DOI: 10.1148/radiol.2313031391]

27 **Zakian KL**, Eberhardt S, Hricak H, Shukla-Dave A, Kleinman S, Muruganandham M, Sircar K, Kattan MW, Reuter VE, Scardino PT, Koutcher JA. Transition zone prostate cancer: metabolic characteristics at 1H MR spectroscopic imaging--initial results. *Radiology* 2003; **229**: 241-247 [PMID: 12920178]

28 **Meirelles GS**, Schöder H, Ravizzini GC, Gönen M, Fox JJ, Humm J, Morris MJ, Scher HI, Larson SM. Prognostic value of baseline

[18F] fluorodeoxyglucose positron emission tomography and 99mTc-MDP bone scan in progressing metastatic prostate cancer. *Clin Cancer Res* 2010; **16**: 6093-6099 [PMID: 20975102 DOI: 10.1158/1078-0432.CCR-10-1357]

29 **Aihara M**, Wheeler TM, Ohori M, Scardino PT. Heterogeneity of prostate cancer in radical prostatectomy specimens. *Urology* 1994; **43**: 60-66; discussion 66-67 [PMID: 8284886]

30 **Bauer DE**, Hatzivassiliou G, Zhao F, Andreadis C, Thompson CB. ATP citrate lyase is an important component of cell growth and transformation. *Oncogene* 2005; **24**: 6314-6322 [PMID: 16007201 DOI: 10.1038/sj.onc.1208773]

31 **Desouki MM**, Geradts J, Milon B, Franklin RB, Costello LC. hZip2 and hZip3 zinc transporters are down regulated in human prostate adenocarcinomatous glands. *Mol Cancer* 2007; **6**: 37 [PMID: 17550612 DOI: 10.1186/1476-4598-6-37]

32 **Franklin RB**, Feng P, Milon B, Desouki MM, Singh KK, Kajdacsy-Balla A, Bagasra O, Costello LC. hZIP1 zinc uptake transporter down regulation and zinc depletion in prostate cancer. *Mol Cancer* 2005; **4**: 32 [PMID: 16153295]

33 **Halliday KR**, Fenoglio-Preiser C, Sillerud LO. Differentiation of human tumors from nonmalignant tissue by natural-abundance 13C NMR spectroscopic. *Magn Reson Med* 1988; **7**: 384-411 [PMID: 2459580]

34 **Hatzivassiliou G**, Zhao F, Bauer DE, Andreadis C, Shaw AN, Dhanak D, Hingorani SR, Tuveson DA, Thompson CB. ATP citrate lyase inhibition can suppress tumor cell growth. *Cancer Cell* 2005; **8**: 311-321 [PMID: 16226706 DOI: 10.1016/j.ccr.2005.09.008]

35 **Trotman LC**, Niki M, Dotan ZA, Koutcher JA, Di Cristofano A, Xiao A, Khoo AS, Roy-Burman P, Greenberg NM, Van Dyke T, Cordon-Cardo C, Pandolfi PP. Pten dose dictates cancer progression in the prostate. *PLoS Biol* 2003; **1**: E59 [PMID: 14691534]

36 **Manning BD**, Cantley LC. AKT/PKB signaling: navigating downstream. *Cell* 2007; **129**: 1261-1274 [PMID: 17604717 DOI: 10.1016/j.cell.2007.06.009]

37 **Plas DR**, Thompson CB. Akt-dependent transformation: there is more to growth than just surviving. *Oncogene* 2005; **24**: 7435-7442 [PMID: 16288290 DOI: 10.1038/sj.onc.1209097]

38 **Calera MR**, Martinez C, Liu H, Jack AK, Birnbaum MJ, Pilch PF. Insulin increases the association of Akt-2 with Glut4-containing vesicles. *J Biol Chem* 1998; **273**: 7201-7204 [PMID: 9516411]

39 **Majewski N**, Nogueira V, Bhaskar P, Coy PE, Skeen JE, Gottlob K, Chandel NS, Thompson CB, Robey RB, Hay N. Hexokinase-mitochondria interaction mediated by Akt is required to inhibit apoptosis in the presence or absence of Bax and Bak. *Mol Cell* 2004; **16**: 819-830 [PMID: 15574336 DOI: 10.1016/j.molcel.2004.11.014]

40 **Berwick DC**, Hers I, Heesom KJ, Moule SK, Tavare JM. The identification of ATP-citrate lyase as a protein kinase B (Akt) substrate in primary adipocytes. *J Biol Chem* 2002; **277**: 33895-33900 [PMID: 12107176 DOI: 10.1074/jbc.M204681200]

41 **Pierce MW**, Palmer JL, Keutmann HT, Hall TA, Avruch J. The insulin-directed phosphorylation site on ATP-citrate lyase is identical with the site phosphorylated by the cAMP-dependent protein kinase in vitro. *J Biol Chem* 1982; **257**: 10681-10686 [PMID: 6286669]

42 **Bandyopadhyay S**, Pai SK, Watabe M, Gross SC, Hirota S, Hosobe S, Tsukada T, Miura K, Saito K, Markwell SJ, Wang Y, Huggenvik J, Pauza ME, Iiizumi M, Watabe K. FAS expression inversely correlates with PTEN level in prostate cancer and a PI 3-kinase inhibitor synergizes with FAS siRNA to induce apoptosis. *Oncogene* 2005; **24**: 5389-5395 [PMID: 15897909 DOI: 10.1038/sj.onc.1208555]

43 **Edinger AL**, Thompson CB. Akt maintains cell size and survival by increasing mTOR-dependent nutrient uptake. *Mol Biol Cell* 2002; **13**: 2276-2288 [PMID: 12134068 DOI: 10.1091/mbc.01-12-0584]

44 **Kawauchi K**, Araki K, Tobiume K, Tanaka N. p53 regulates glucose metabolism through an IKK-NF-kappaB pathway and inhibits cell transformation. *Nat Cell Biol* 2008; **10**: 611-618 [PMID: 18391940 DOI: 10.1038/ncb1724]

45 **Morris MJ**, Akhurst T, Larson SM, Ditullio M, Chu E, Siedlecki K, Verbel D, Heller G, Kelly WK, Slovin S, Schwartz L, Scher HI. Fluorodeoxyglucose positron emission tomography as an outcome measure for castrate metastatic prostate cancer treated with antimicrotubule chemotherapy. *Clin Cancer Res* 2005; **11**: 3210-3216 [PMID: 15867215 DOI: 10.1158/1078-0432.CCR-04-2034]

46 **Bahri H**, Laurence L, Edeline J, Leghzali H, Devillers A, Raoul JL, Cuggia M, Mesbah H, Clement B, Boucher E, Garin E. High prognostic value of 18F-FDG PET for metastatic gastroenteropancreatic neuroendocrine tumors: a long-term evaluation. *J Nucl Med* 2014; **55**: 1786-1790 [PMID: 25286923 DOI: 10.2967/jnumed.114.144386]

47 **Binderup T**, Knigge U, Loft A, Federspiel B, Kjaer A. 18F-fluorodeoxyglucose positron emission tomography predicts survival of patients with neuroendocrine tumors. *Clin Cancer Res* 2010; **16**: 978-985 [PMID: 20103666 DOI: 10.1158/1078-0432.CCR-09-1759]

48 **Noy A**, Schöder H, Gönen M, Weissler M, Ertelt K, Cohler C, Portlock C, Hamlin P, Yeung HW. The majority of transformed lymphomas have high standardized uptake values (SUVs) on positron emission tomography (PET) scanning similar to diffuse large B-cell lymphoma (DLBCL). *Ann Oncol* 2009; **20**: 508-512 [PMID: 19139176 DOI: 10.1093/annonc/mdn657]

49 **Robbins RJ**, Wan Q, Grewal RK, Reibke R, Gonen M, Strauss HW, Tuttle RM, Drucker W, Larson SM. Real-time prognosis for metastatic thyroid carcinoma based on 2-[18F]fluoro-2-deoxy-D-glucose-positron emission tomography scanning. *J Clin Endocrinol Metab* 2006; **91**: 498-505 [PMID: 16303836 DOI: 10.1210/jc.2005-1534]

P- Reviewer: Hekal IA, Huang SP, Simone G **S- Editor**: Ji FF
L- Editor: A **E- Editor**: Li D

Published by **Baishideng Publishing Group Inc**
8226 Regency Drive, Pleasanton, CA 94588, USA
Telephone: +1-925-223-8242
Fax: +1-925-223-8243
E-mail: bpgoffice@wjgnet.com
Help Desk: http://www.wjgnet.com/esps/helpdesk.aspx
http://www.wjgnet.com